Journal of Nuclear Materials 390–391 (2009) 826–829

Contents lists available at ScienceDirect

Journal of Nuclear Materials

journal homepage: www.elsevier.com/locate/jnucmat

Whole device ELM simulations

D.P. Coster

Max-Planck-Institut für Plasmaphysik, EURATOM Association, Boltzmannstr 2, Garching bei Muenchen D85748, Germany

ARTICLE INFO

PACS:
52.65.Kj
52.65.Pp
52.25.Fi

ABSTRACT

A simple ELM model is used in the SOLPS fluid-plasma, Monte-Carlo neutrals code with a grid that encompasses the core and Scrape-Off Layer. Sources in the core are prescribed based on previous work done with a 1d core transport code, and with the transport coefficients varied to produce a reasonable match to a particular ASDEX Upgrade discharge. Time-dependent calculations were then performed that looked at the effect of changing the ELM magnitude and radial extent (keeping the ELM frequency and duration fixed) and of varying the upstream separatrix density using a local gas puff under feed-back control to prescribe the density.

1. Introduction

SOLPS [1] (and references therein), the combination of a fluid-plasma code, B2, and a Monte-Carlo neutrals code, Eirene, has been used to examine the effects of ELMs on a plasma. For these simulations, a grid based on an ASDEX Upgrade discharge has been used [2], with a grid that encompasses most of the core, in addition to the Scrape-Off Layer. Sources arising from neutral beam injection were used based on an ASTRA [3] simulation of the discharge and transport coefficients were chosen to give a reasonable match to the chosen discharge, Fig. 1. The main thrust of this work was not to model any particular discharge (this has been done for this particular discharge, see [4,5]) but to look at the effects of differences in the ELM model on the whole plasma, including the core. A series of extended code runs were performed where the depth and magnitude of the ELM was varied and (separately) the separatrix density was varied. Some additional runs were performed to explore time dependence in the Monte-Carlo treatment of neutrals, and on the effect of ELMs on the plate temperature.

In the next section, the particulars of the simulations are outlined and the results presented. In the following section, the results of some 1d (parallel) simulations are presented and the paper concludes with a discussion and some conclusions.

2. Deep simulations

In previous work, a radial transport profile was found that, in combination with a radial profile of sources arising from NBI, reasonably reproduced the basic characteristics of an H-mode AUG plasma. In these simulations, done with a fluid-plasma and kinetic neutrals treating D + C + He, the ELMs were simulated by adding an additional component to the transport profiles, Fig. 2. The basic ELM was achieved with an additional factor of 10 enhancement of the transport coefficients starting from 2 cm inside the separatrix (measured at the outer midplane) extending over the whole SOL (a little more than 3 cm). For this study, no poloidal enhancement was done. The ELM was switched on for 200 μs and occurred every 5 ms. This model was used to perform a density scan where a gas puff was used under feed-back control to set the separatrix density (from the base case of 1.5×10^{19} m^{-3} to 2.0, 2.5, 3.0 and 4.0×10^{19} m^{-3}). (For comparison, runs were also performed without ELMs.) Then at the base density, the effects of increasing the depth (to 5 cm and 10 cm) of the ELM affected region was explored, and also the 'strength' of the ELM by increasing the transport enhancement factor (31 times and 100 times). For the base case, thermal simulations of the targets were also performed. A time-step for the plasma code (B2) of 1×10^{-5} s was used for all cases, and just short of 2 s of plasma time was simulated (representing a bit more than half a year of cpu time per simulation). For these simulations, the neutrals were run with a time-step of 1 s in Eirene (comparisons with cases using the same time-step for the neutrals as the plasma showed no difference – see Fig. 4).

Fig. 3 shows the comparison of the electron temperature and density profiles for the density scan cases with and without ELMs. For the lowest density case (1.5×19^{19} m^{-3}), it can be seen that there is a strong effect on the global electron temperature profile, but not on the density profile. For the highest density case (4×19^{19} m^{-3}), the situation is reversed – the global temperature profile is only slightly affected, while the global density profile is affected. For these cases, the profiles for the ELM cases are plotted just before the next ELM cycle (4.9 ms/4.7 ms after the start/end of the previous ELM and 0.1 ms before the next ELM), and enough time had passed that the profiles were no longer evolving on the

E-mail address: David.Coster@ipp.mpg.de

0022-3115/$ - see front matter © 2009 Published by Elsevier B.V.
doi:10.1016/j.jnucmat.2009.01.218

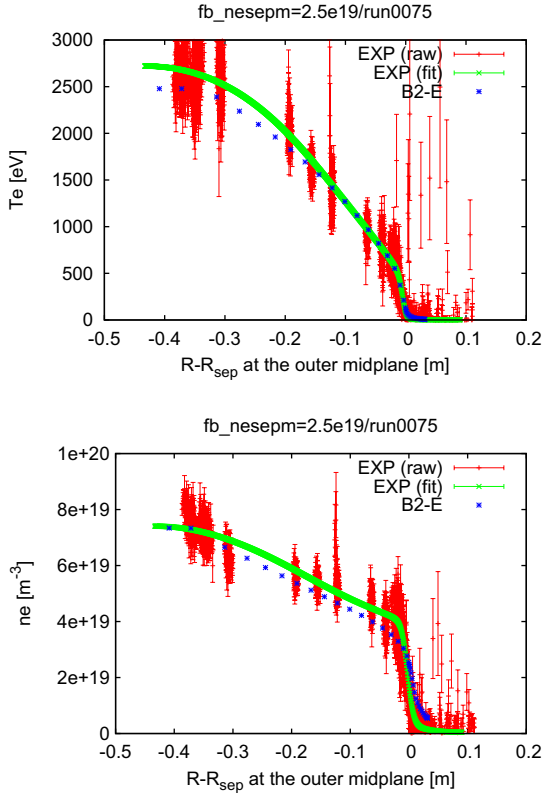

Fig. 1. Comparison of the 2.5×10^{19} m^{-3} separatrix density noELM simulation with AUG shot 17151 (0.8 MA, 2 T) in the time window 3.5–4.2 s.

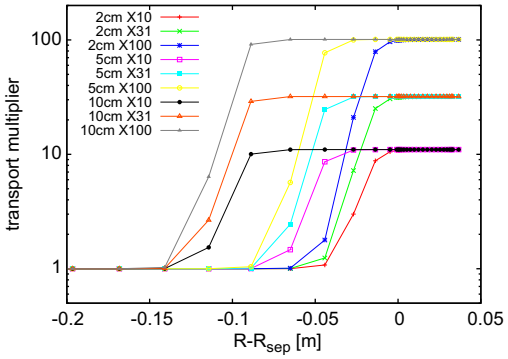

Fig. 2. Multipliers for the transport coefficients for the 2 cm, 5 cm and 10 cm depths and ×10, ×31 and ×100 'strengths' used for the ELM simulations.

longer time-scale. Table 1 gives the size of the ELM in terms of the difference of the core energy content just before and just after the ELM – for these cases the ELM losses are almost identical. Fig. 4 shows the power reaching the targets for the density scan cases.

In the 'depth' and 'strength' scan, two effects can be distinguished: the effect on the size of the ELM and the effect on the total plasma (compared to the no ELM case). Table 2 gives the ELM sizes for the ELM 'depth' and 'strength' scan – the depth does not seem to have a large effect on the ELM size, but, as seen in Table 3 (where the stored energy normalised to the no ELM case is given), does affect the plasma energy content. The power to the targets is shown in Fig. 5.

For the base case, runs were also done with the thermal plate model enabled [6]. Fig. 6 shows the increase of the plate temperature with time at a number of positions on the plate for the case without and with ELMs. The ELM case shows the affect of individ-

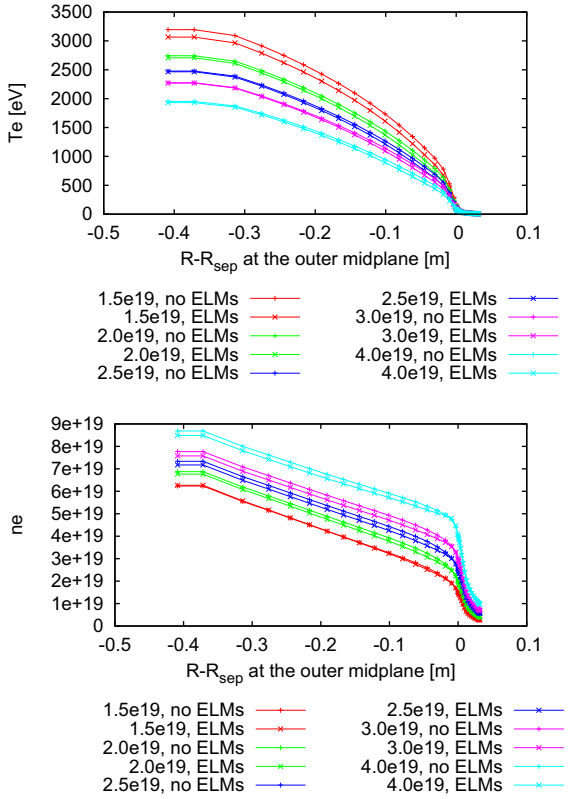

Fig. 3. Comparison of the Te (upper) and ne (lower) profile for simulations with and without ELMs.

Table 1
ELM energy drop, ΔE_{ELM}, for the 2 cm, ×10 density scan.

Density (10^{19}) m^{-3}	ΔE_{ELM} (kJ)
1.5	3.462
2.0	3.548
2.5	3.554
3.0	3.549
4.0	3.475

Table 2
ELM energy drop, ΔE_{ELM}, for the 1.5×10^{19} m^{-3} ELM strength scan.

Depth (cm)	ΔE_{ELM} (kJ)		
	Transport multiplier		
	×10	×31	×100
2	3.462	6.635	10.277
5	3.900	7.595	11.473
10	3.871	7.483	11.410

Table 3
Fraction of the total stored energy for the ELM cases (taken just before the start of the next ELM) compared to the stored energy of the no ELM case, E_{ELM}/E_{noELM}.

Depth (cm)	E_{ELM}/E_{noELM}		
	Transport multiplier		
	×10	×31	×100
2	0.94	0.88	0.79
5	0.89	0.78	0.65
10	0.82	0.65	0.48

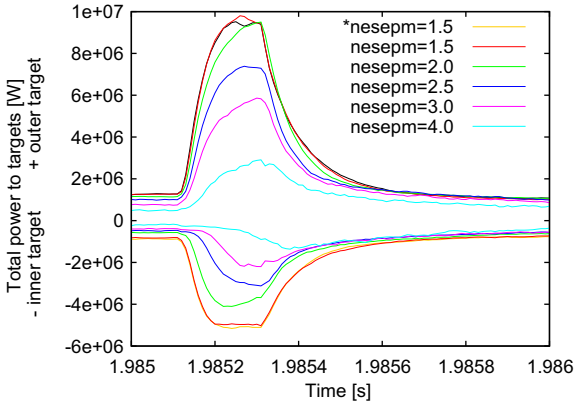

Fig. 4. Comparison of total power to the outer (positive) and inner (negative) targets for the density scan cases. The '*nesepm = 1.5' case used the same time-step of 10 μs for both B2 and EIRENE.

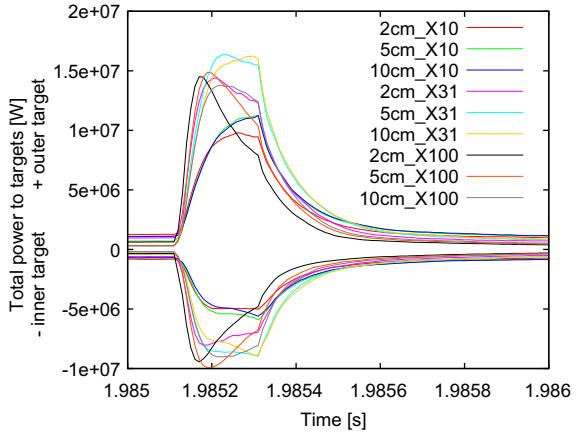

Fig. 5. Comparison of total power to the outer (positive) and inner (negative) targets for the 'depth' and 'strength' scan cases.

ual ELMs as well – relatively small in this case. Fig. 7 compares the plate temperature at the same time point for the two cases – the most pronounced effect of the ELMs has been to slightly broaden the power deposition profile, lowering the peak plate temperature.

3. One dimensional (parallel) simulations

On a side-note, some 1d (parallel) simulations were also performed (D only, with a fluid neutral model, and a time-step in B2 of 0.1 μs). These demonstrated a bifurcation in the solutions, with two solutions possible over a range of 'upstream' densities. In the 'hot' branch, indicated by squares in Fig. 8, the volume integral of the ionization equals the target recycling flux. For the 'cold' branch, the target flux is essentially negligible, and the volume ionization flux is balanced by the volume recombination flux. For a range of upstream separatrix densities two solutions are found, depending on whether the simulations were started from a 'hot' or 'cold' case. Fig. 9 shows the effect of applying a heat pulse ('ELM') at the left boundary to one of the 'hot' solution cases. The propagation of the heat pulse towards the target can be clearly seen.

4. Summary and outlook

This work has explored the effect of ELMs on the whole plasma using a simulation domain that encompasses almost all of the core and the Scrape-Off Layer. At higher densities, the ELMs seem to

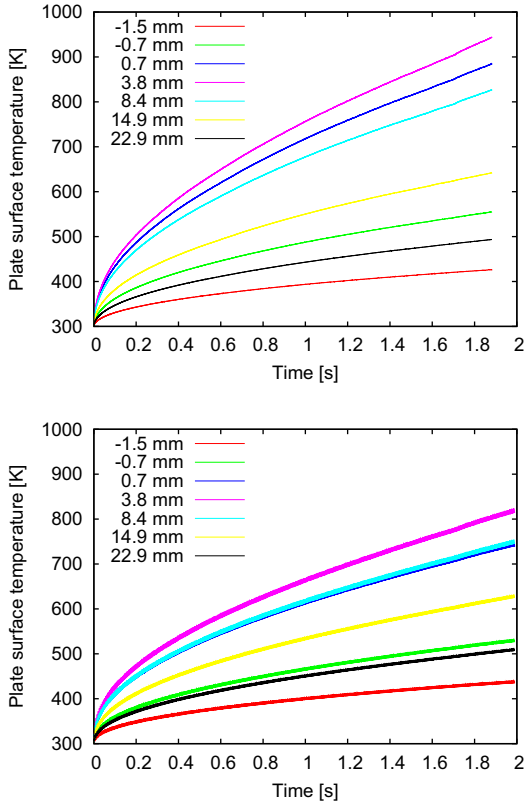

Fig. 6. Outer target plate temperatures as a function of time for various positions for the case without (upper) and with (lower) ELMs. The thicker lines in the lower graph is due to the individual ELMs – a zoom is shown in Fig. 7.

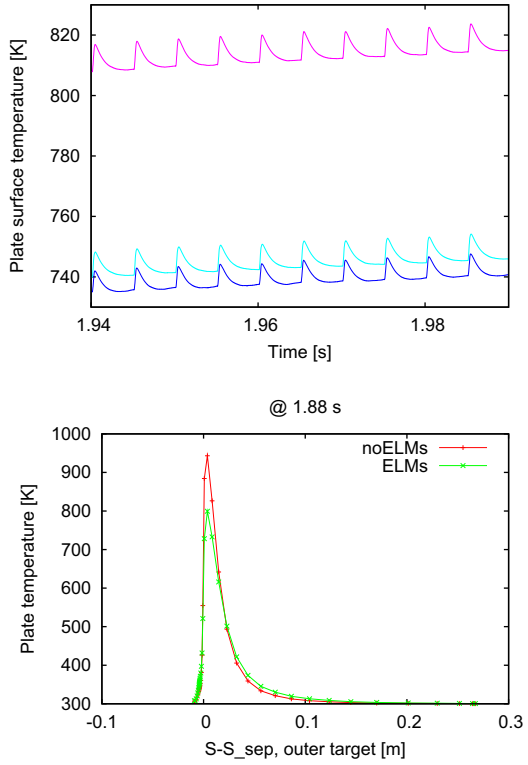

Fig. 7. Top: zoom of the lower graph in Fig. 6 with the same color coding. Bottom: outer target plate temperatures as a function of position along the outer target at 1.88 s, with and without ELMs.

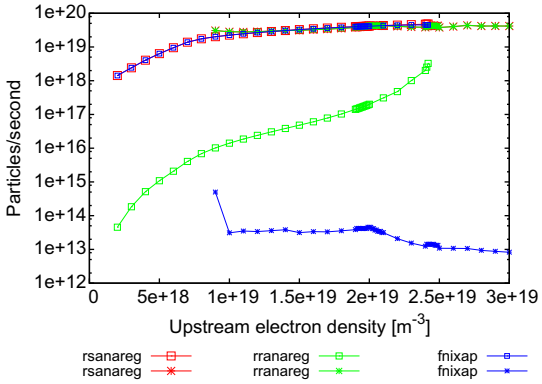

Fig. 8. Volume integral of the ionization ("rsanareg"), volume integral of the recombination ('rranareg') and surface integral of the target fluxes ("fnixap"). Squares represent the'hot' branch, stars represent the 'cold' branch.

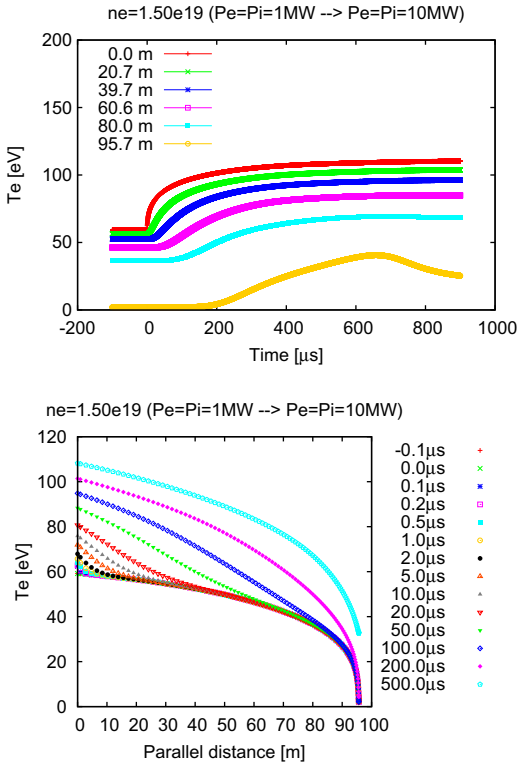

Fig. 9. Profiles of Te for a 1d ELM case where the power was increased from 2 MW to 20 MW. In the upper graph, the ELM starts at 0.0 μs, and each line shows Te as a function of time starting from the source region (0.0 m) to the target (95.7 m). In the lower graph, profiles of Te as a function of parallel distance are shown at particular times.

affect the global density profile, while having little affect on the global temperature profile. For lower density cases, the situation is reversed: the global temperature profile is affected while the global density profile is little changed.

While the approach used here for the whole plasma ELM simulations represents probably the best that can be done with a 2d transport code, it does not really represent a feasible method for routine analysis. More than 10 cpu years have been used for these runs, with an elapsed time of more than half a year.

Three approaches for core-edge coupling can be envisioned: **mediated**, where the edge codes are used to provide boundary conditions for the core codes on the basis of fitting coefficients to the results of a number of edge runs; **direct** where the edge and core codes are directly coupled; and **avoided** where (as here) the edge code is extended all the way to the centre of the plasma. The first method will always be significantly faster than the other two methods, but probably the least accurate – particularly in time-dependent situations such as the ELM case. The other two methods are likely to be similar in speed, since the cost will always be dominated by the 2d component. It seems likely that some combination of the three techniques will continue to be used.

References

[1] R. Schneider, X. Bonnin, K. Borrass, D.P. Coster, H. Kastelewicz, et al., Contrib. Plasma Phys. 46 (2006) 3, doi:10.1002/ctpp.200610001.
[2] C. Konz, D.P. Coster, K. Lackner, G. Pautasso, ASDEX Upgrade Team, in: C. Hidalgo, B.P. van Milligen (Eds.), Europhysics Conference Abstracts (CD-ROM, Proceedings of the 32nd EPS Conference on Plasma Physics, Tarragona, 2005), vol. 29C, EPS, Geneva, 2005, p. O-2.005.
[3] G. Pereverzev, P. Yushmanov, IPP-Report IPP 5/98, Max-Planck Institute fur Plasmaphysik, 2002.
[4] L.D. Horton, A.V. Chankin, Y.P. Chen, G.D. Conway, D.P. Coster, et al., Nucl. Fus. 45 (2005) 856.
[5] A.V. Chankin, D.P. Coster, R. Dux, C. Fuchs, G. Haas, et al., Plasma Phys. Control. Fus. 48 (2006) 839.
[6] D. Coster, X. Bonnin, G. Corrigan, R. Dejarnac, M. Fenstermacher, et al., J. Nucl. Mater. 313–316 (2003) 868.